AIP | The Journal of Chemical Physics

Ultrafast photo-induced nuclear relaxation of a conformationally disordered conjugated polymer probed with transient absorption and femtosecond stimulated Raman spectroscopies

Wenjian Yu, Paul J. Donohoo-Vallett, Jiawang Zhou, and Arthur E. Bragg

Citation: The Journal of Chemical Physics **141**, 044201 (2014); doi: 10.1063/1.4890326
View online: http://dx.doi.org/10.1063/1.4890326
View Table of Contents: http://scitation.aip.org/content/aip/journal/jcp/141/4?ver=pdfcov
Published by the AIP Publishing

Ultrafast photo-induced nuclear relaxation of a conformationally disordered conjugated polymer probed with transient absorption and femtosecond stimulated Raman spectroscopies

Wenjian Yu, Paul J. Donohoo-Vallett, Jiawang Zhou, and Arthur E. Bragg[a)]
Department of Chemistry, Johns Hopkins University, 3400 N. Charles St., Baltimore, Maryland 21218, USA

(Received 9 May 2014; accepted 2 July 2014; published online 29 July 2014)

A combination of transient absorption (TAS) and femtosecond stimulated Raman (FSRS) spectroscopies were used to interrogate the photo-induced nuclear relaxation dynamics of poly(3-cyclohexyl,4-methylthiophene) (PCMT). The large difference in inter-ring dihedral angles of ground and excited-state PCMT make it an ideal candidate for studying large-amplitude vibrational relaxation associated with exciton trapping. Spectral shifting in the S_1 TA spectra on sub-ps timescales (110 ± 20 and 800 ± 100 fs) is similar to spectroscopic signatures of excited-state relaxation observed with related photoexcited conjugated polymers and which have been attributed to exciton localization and a combination of resonant energy transfer and torsional relaxation, respectively. Measurements made with both techniques reveal fast PCMT S_1 decay and triplet formation ($\tau_{S1} = 25$–32 ps), which is similar to the excited-state dynamics of short oligothiophenes and highly twisted polyconjugated molecules. On ultrafast timescales FSRS of S_1 PCMT offers a new perspective on the nuclear dynamics that underlie localization of excitons in photoexcited conjugated polymers: Spectral dynamics in the C=C stretching region (1400–1600 cm^{-1}) include a red-shift of the in-phase C=C stretching frequency, as well as a change in the relative intensity of in-phase and out-of-phase stretch intensities on a timescale of ∼100 fs. Both changes indicate an ultrafast vibrational distortion that increases the conjugation length in the region of the localized excitation and are consistent with exciton self-localization or trapping. Wavelength-dependent excited-state FSRS measurements further demonstrate that the C=C stretching frequency provides a useful spectroscopic handle for interrogating the degree of delocalization in excited conjugated polymers given the selectivity achieved via resonance enhancement. © *2014 AIP Publishing LLC*. [http://dx.doi.org/10.1063/1.4890326]

I. INTRODUCTION

Conjugated polymers have become a common component in organic electronic material[1,2] and there is continued interest in characterizing properties and dynamics of the electronic states that underlie their material behaviors.[3–13] On a fundamental level conjugated polymers raise interesting questions regarding the nature of localized states in disordered, highly inhomogeneous systems and also regarding what structural changes are responsible for trapping these states along an extended π-conjugated framework.[14–16] The structural complexity of these systems leads naturally to many questions: How does one accurately describe delocalized states on a disordered polymer backbone?[14] How are the properties of polymer excitations determined by both the polymer's torsional conformation and other structural variations along the polymer backbone? What structural relaxation dynamics following photoexcitation are responsible for exciton trapping and how can we observe such nuclear evolution directly?[7,17] Addressing these questions experimentally requires methods that can differentiate amongst structural variations within an ensemble of localized excited states and track excited-state structural relaxation directly in time.[7,12] Here we specifically demonstrate the use of femtosecond stimulated Raman spectroscopy (FSRS)[18] in combination with ultrafast transient absorption spectroscopy (TAS) to characterize the nuclear relaxation associated with exciton trapping in the conjugated polymer poly(3-cyclohexyl,4-methylthiophene), or PCMT.

The photoinduced dynamics and spectroscopy of conjugated polymers in solution have been examined extensively over the last decade using various transient electronic spectroscopies in order to address the questions listed above.[3–13] From these studies it has been concluded that the dynamics underlying various phases of excited-state relaxation include: (1) Exciton self-trapping or localization, associated with transient spectral evolution over timescales of ∼100 fs or less;[3–5,7,9,10] (2) Resonant excitonic energy transfer (EET)[3,6,11,19] through which energy migrates to lower-energy sites characterized by different degrees of delocalization and/or (3) local, long-range torsional relaxation, both occurring on timescales ranging from sub-ps to 10 s of ps;[4,5,9,10,12] and, (4) singlet exciton decay by emission and intersystem crossing (ISC), occurring on timescales of 100 s of picoseconds.[3,12,13] ISC is readily identified by the appearance of a triplet absorption band at slightly higher transition energies, analogous to the spectral dynamics of conjugated oligomers.[12,20,21] Signatures of EET have been identified through measurements of both time-dependent

a)Electronic mail: artbragg@jhu.edu.

spectral diffusion[8] and anisotropy depolarization;[3,8,11] the latter have revealed very fast and appreciable randomization of the stimulated emission (or fluorescence) polarization after excitation, which models predict to occur primarily via energy transfer between sites.[11,22,23] The relative importance of EET and torsional relaxation has been debated for some time, but pump-probe (transient absorption and time-resolved fluorescence),[4,11] multi-pulse,[4] and photon-echo spectroscopies[9] have shed new light on the relaxation dynamics of polythiophenes in recent years, revealing that local relaxation contributes significantly to the stabilization of excited poly(3-alkylthiophenes). Although nuclear relaxation associated with exciton self-trapping is the most plausible explanation for transient evolution in the electronic spectroscopy of excited polymers on ultrafast timescales,[4,9] there is little information about what occurs during this process directly from experiment. This can be attributed to the very fast timescale on which localization occurs, as well as the fact that clear spectroscopic interrogation of this localization requires a sensitive probe of ultrafast nuclear dynamics out of the Franck-Condon region in the excited state.[9]

Raman spectroscopy has been used extensively to characterize conjugated polymers and polymer-based materials,[24–31] and is a promising complement to electronic spectroscopies for interrogating the structural characteristics and dynamics of conjugated polymers in their excited states.[7,12] Conjugated polymers and oligomers exhibit very large ground-state Raman cross-sections, with spectra dominated by totally symmetric modes that coincide with the change in molecular geometry that accompanies polymer excitation.[32] Furthermore, vibrational frequencies of various Raman-active modes (most notably the in-phase C=C stretching frequency) are directly sensitive to the extent of delocalization along an oligomer or polymer backbone.[32,33] Given that excited states of conjugated oligomers and polymers are highly delocalized by nature, we anticipate that C=C stretching frequencies of excited states should be highly sensitive to variations or evolution in the excited-state delocalization length. Thus, time-resolved excited-state Raman spectroscopy could be used as a direct method for interrogating evolution in conformation and delocalization length that occurs through the course of excited-state relaxation of photoexcited conjugated polymers and oligomers.[12]

In previous work we used time-resolved resonant FSRS to investigate the picosecond structural relaxation dynamics of regio-regular poly(3-hexylthiophene) (RR-P3HT) following photoexcitation at 510 nm.[12] Time-dependent evolution in the excited-state Raman spectrum on a timescale of 9 ps was attributed to the influence of conformational relaxation on the resonant enhancement of modes that involve moieties within the conjugated backbone; this behavior was explained to result from torsion-induced changes to the Franck-Condon overlap between the excited and probing states, and occurs on a similar timescale as spectral relaxation in near-IR absorption transients. Raman measurements also revealed a feature between 1300 and 1350 cm^{-1} that only evolved with the population decay of the excited state; we attributed this feature to vibrations peripheral to the conjugated backbone that effectively spectate conformational relaxation, and we postulated that this feature corresponds with modes localized around polymer defects or distortions that demarcate the boundaries of localized excited states. Thus, this work demonstrated that excited-state Raman spectroscopy can offer new and more detailed perspective on the structural properties and dynamics of photoexcited polymers and complements what can be gleaned from transient electronic spectroscopies.

Here we further explore the use of FSRS for interrogating the vibrational spectroscopy and dynamics of conjugated polymers, and specifically those of PCMT. We use the ultrafast evolution in the frequencies and band shapes in the C=C stretching region as a probe of the initial nuclear relaxation dynamics associated with exciton trapping, making use of the high time resolution available with FSRS.[18] The substitution pattern along the conjugated backbone in PCMT gives rise to very large inter-ring dihedral angles compared to other polythiophenes in their ground states, and we expected that TAS and FSRS should be particularly sensitive to large-amplitude twisting or deformation along these angles as PCMT relaxes out of the Franck-Condon region in the S_1 state. We have also interrogated the structural dependence of intersystem crossing (ISC) on longer picosecond timescales. Finally, the spectroscopic selectivity of wavelength-dependent resonantly enhanced FSRS enables characterization of the variations in delocalization that underlie broad transient electronic absorption bands of the excited polymer.

II. EXPERIMENTAL METHODS

A. Sample preparation

PCMT and RR-P3HT (electronic grade, molecular weight 50–70 kD) were purchased from Rieke metals and used "as-is" after prolonged purging with high-purity dry argon. Chlorobenzene (CB, Fisher Scientific, >99% purity) and unstabilized tetrahydrofuran (THF, Sigma Aldrich, >99.9% purity) were deaerated through repeated freeze-pump-thaw cycles using liquid nitrogen. Under an argon atmosphere, solutions of PCMT in THF and RR-P3HT in CB were prepared in vials and transferred into the reservoir of a sample flow loop. Spectroscopic measurements were made on sample solutions as they passed through a flow cell with a 0.5 mm pathlength and fused-silica windows (Spectrocell). The sample flow circuit was constructed entirely of PTFE tubing and compression fittings to ensure chemical compatibility with the solvents used and has a circulation volume of less than 30 ml. Samples were circulated at 15 ml/min with a peristaltic pump during the course of spectroscopic measurements, and no signs of photoproduct were observed after many hours of exposure to laser pulses.

Higher sample concentrations (1 mg/ml) were necessary for conducting excited-state Raman measurements, whereas lower sample concentrations (0.2 mg/ml) were used for transient absorption measurements and ground-state Raman measurements with P3HT. We have previously demonstrated that the photophysics of P3HT does not change within this concentration range.[12] We likewise observe no differences in the photophysics of PCMT at low and high sample concentrations. PCMT samples used for TAS measurements had an OD

of 0.5 at the excitation wavelength; the OD used for FSRS measurements was much higher (>2).

Steady-state UV-Vis spectra of sample solutions were measured using a diode-array spectrometer fiber-optically coupled to incandescent deuterium and tungsten light sources (Stellarnet). Samples used for measurements of steady-state absorption spectra were diluted to have OD < 1 in a 0.5 mm cuvette at the peak absorption wavelength.

B. Laser instrumentation and measurements

Steady-state resonant Raman measurements with ground-state polymer in solution were conducted using FSRS.[18] Excited-state polymer spectroscopy and dynamics were examined using broadband TAS and time-resolved FSRS. All measurements utilized ultrafast laser pulses, which were derived from the fundamental output of an amplified Ti:Sapphire laser (Coherent Legend Elite, 4.5 mJ/pulse, 1 kHz rep. rate, 35-fs pulse duration, 800-nm peak wavelength). Half of this output was used to pump an optical parameteric amplifier (Coherent OperaSolo) that generates photoexcitation pulses (or actinic pulses) at 320 nm through second harmonic generation of the second harmonic of the OPA signal at 1280 nm; excitation pulses were attenuated to an energy of 3 μJ/pulse for these measurements. Another portion of the amplifier output (~1 mJ/pulse) was used to pump a second-harmonic bandwidth compressor (SHBC, Light Conversion), which generates narrowband (~12 cm^{-1}) pulses with 2–3 ps duration at 400 nm. Pulses derived from the SHBC were used either directly for ground-state stimulated Raman measurements or to pump a white-light-seeded OPA (TOPAS-400, Light Conversion) in order to generate tunable narrowband Raman-excitation (or Raman-pump) pulses for wavelength-dependent excited-state and transient Raman experiments (600 nm or 840 nm). The Raman-pump pulse energy was typically 10–15 μJ/pulse. A few μJ of amplifier output at 800 nm was focused into a 2-mm-thick sapphire crystal to generate a broadband probe continuum used in all measurements (420–720 nm or 850–1100 nm).

Photoexcitation pulses (or actinic pulses, at 320 nm) were focused to a 2-mm beam diameter on the sample. Raman-excitation pulses were focused towards the sample with a 1-m focal-length lens, with the focus located behind the sample; the Raman-excitation beam had a 500 μm diameter at the position of the sample and crossed at the center of the larger beam profile of the actinic pump. White-light probing pulses were focused to the center of the Raman-pump beam on the sample with a ~50 μm diameter using an off-axis parabolic mirror. The sizes, pulse energy and overlap of the three beams guarantee the collection of three-pulse signals, and specifically excited-state Raman spectra via FSRS.

Photoexcitation and Raman-pump pulses were blocked after the sample with a set of long-pass filters, and probe pulses were collected and dispersed with a 300-mm spectrograph (Acton-2360) onto a CCD camera (Pixis-100BR). The camera was configured to collect spectra at the laser's repetition rate, with the photoexcitation beam and Raman beam chopped (or blocked) accordingly for each type of measurement. The output reference signals from both the camera and the choppers were used to correlate chopper phases with each exposure.

Multiple types of measurements were made using this optical configuration:[34]

(1) Broadband TAS probing at visible (420–750 nm) and near-IR wavelengths (830–1100 nm) was conducted by blocking the Raman excitation beam and chopping the photoexcitation beam at one half of the laser repetition rate. Transient spectra were computed with white-light spectra (photoexcitation on vs. off) from consecutive laser shots dispersed across the detector array using a low-resolution grating (800-nm blaze, 150 lines/mm).
(2) Ground-state Raman (GSR) measurements were made by blocking the photoexcitation beam and chopping the Raman-excitation beam. GSR spectra were likewise computed from a comparison of consecutive white-light spectra (Raman excitation on vs. off) dispersed at much higher resolution (grating: 1000-nm blaze, 600 lines/mm). Linewidths in these measurements were limited predominantly by the bandwidth of the Raman excitation source (15–20 cm^{-1}), as well as natural transition linewidths, spectral congestion, and spectral inhomogeneity.
(3) Three-pulse transient and excited-state Raman measurements were conducted using a four-phase chopping sequence, with the photoexcitation and Raman excitation beams chopped at one-fourth and one-half of the laser repetition rate, respectively (Photoexcitation/Raman-excitation sequences: on/on; on/off; off/on; off/off). Multiple signals were derived simultaneously with this approach, including: TAS covering the spectral region probed in Raman measurements (on/off vs. off/off); GSR (off/on vs. off/off); and three-pulse signals collected in the presence of the photoexcitation pulse (on/on vs. on/off). For brevity, we refer to the third signal as Raman-excitation chopped (RC), although GSR and other (non-Raman) three-pulse signals also appear in these spectra (see Sec. II C below). A complementary three-pulse signal can be obtained by synchronously chopping (SC) both beams (on/on vs. off/off).

Each of these spectra was calculated from the measurement sequence as follows:

$$\mathrm{TAS} = \log(\mathrm{I_{pu+pr}}/\mathrm{I_{pr}}), \tag{1a}$$

$$\mathrm{GSR} = \log(\mathrm{I_{r+pr}}/\mathrm{I_{pr}}), \tag{1b}$$

$$\mathrm{RC} = \log(\mathrm{I_{pu+r+pr}}/\mathrm{I_{pu+pr}}), \tag{1c}$$

$$\mathrm{SC} = \log(\mathrm{I_{pu+r+pr}}/\mathrm{I_{pr}}). \tag{1d}$$

Subscripts in Eqs. (1a)–(1d) correspond with photoexcitation (pu), Raman excitation (r), and white light probe (pr) pulses, respectively. As described in Sec. II C, we make use of these various signals to isolate excited-state Raman features in our spectral analysis. Each Raman spectrum presented here is an average of 15 000–30 000 measurements cycles (2- or 4-phase).

Timings of the photo- and Raman-excitation pulses relative to the probe pulse were controlled with two motorized translation stages (Newport ESP301-2N and Newport MFA-PPD, respectively). The stages controlling the photoexcitation and Raman time delays were outfitted with a protected silver or aluminum retroreflecting mirrors to ensure that the path of the excitation beam was parallel to the stage. Positioning of the stages, rotation of the spectrograph gratings, collection of spectra, synchronization with choppers, and calculation of transient spectra were all coordinated through a data acquisition program written in LabView.

TAS measurements were conducted with a magic-angle pump-probe polarization. In contrast, polarizations of all three pulses were kept parallel for Raman measurements. For ground-state Raman measurements, the relative Raman pump-probe pulse delay was timed such that the probe pulse arrived near the middle of the Raman pump pulse duration, as it was determined that this gave the best Raman line shapes from the solvent. For excited-state Raman spectra the probe pulse was timed to arrive slightly earlier in the Raman excitation pulse in order to minimize excited-state population depletion induced by the Raman-pump when on resonance.

The time-dependent, two-photon (pump-probe) solvent response of neat THF was used for correcting the influence of temporal chirp from the continuum probe in transient measurements. An example of the time-dependent solvent response and a brief description of chirp correction procedures are provided in the supplementary material.[35] Wavelength-dependent cuts through the solvent response were used to determine the effective time-resolution of the experiment, which was found to range between 100 and 150 fs from the near UV to the near IR.

C. FSRS signal analysis procedures

Three-pulse FSRS spectra contain contributions from multiple spectroscopic signals.[36,37] Steps involved in processing spectra to isolate excited-state Raman features are described below and are illustrated graphically in Figure 1.

Our analysis begins with the synchronously chopped (SC) spectrum (dark-blue curve, Fig. 1), which contains five signal contributions: Solvent and polymer GSR, polymer ESR, Raman-pump induced modulations in transient absorption (TA), and other signals from nonlinear processes. In a first step we remove ground-state Raman signal contributions (dark-yellow curve, Fig. 1). Formally, these should include non-resonant GSR from both solvent and polymer. GSR signals from PCMT are negligible compared to solvent bands at the Raman-excitation wavelengths used in transient measurements,[35] and we therefore assume that pump induced changes in the non-resonant polymer GSR is negligible compared to ESR contributions. We remove GSR contributions from the SC spectra through scaled subtraction; the scaling factor, m, is optimized in order to remove the THF solvent peak appearing at 914 cm^{-1}, specifically.

The difference spectrum (SC-m^*GSR, light-blue curve in Fig. 1) obtained through this procedure contains primarily ESR and broad background signal. Most of the latter originates from Raman-pump-induced depletion of the excited-state transient absorption;[36,37] thus, the TA signal collected simultaneously in this optical window provides a first-order approximation for the shape of the broad baseline and can be used to remove much of the baseline by scaling with an appropriate factor (denoted as k). The result of scaled subtraction of the TA signal is shown in red in Fig. 1. From here we assume that the contribution to the background from other nonlinear processes can be approximated with a polynomial. In total, excited-state Raman spectra were obtained using the formula:

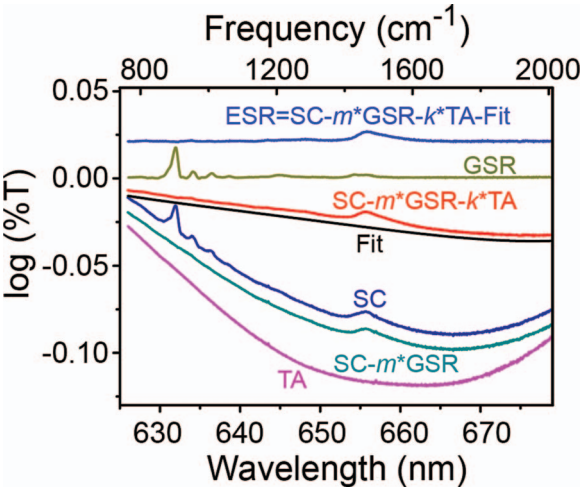

FIG. 1. Representative FSRS data acquired with PCMT and an illustration of spectral analysis for isolating excited-state Raman features. Spectra have been offset for clarity.[35] Transient absorption (TA), ground-state Raman (GSR), and synchronously chopped (SC) signals are obtained experimentally as described in the text. m and k are scalars for subtraction of GSR and TA signals contributing to SC, and "Fit" refers to a polynomial baseline fit applied to account for low-frequency base-line modulation. Procedures for isolating excited-state Raman (ESR) features are outlined in the text.

$$\mathrm{ESR} = \mathrm{SC} - m^*\mathrm{GSR} - k^*\mathrm{TA} - \mathrm{Fit}. \quad (2)$$

Spectral regions where there are no significant ESR signals (below 1150 cm^{-1} or above 1650 cm^{-1}) were utilized to arrive at the best polynomial fit for the residual baseline. The values of k and polynomial parameters that yield the minimum sum of residual squares in these regions were deemed to provide the best baseline correction.

The time-dependent value of m provides an internal standard for the effective Raman-pump intensity and can be used to correct the intensities of ESR features after their isolation. Values of m were found to range between 0.7 and 1 at both Raman probe wavelengths and were used to correct time-resolved FSRS intensities on picosecond timescales. The time-dependent values of k provide a measure of excited-state depopulation induced by interactions with the Raman-excitation pulse. At 840 nm the value of k was found to be roughly constant near 0.85. At 600 nm k started at ~1 and dropped through actinic pump-probe delays that are within the duration of the Raman-excitation pulse, but held between 0.4 and 0.5 on delays of picoseconds to tens of picoseconds. As variation in k suggests variation in excited-state population available to probe by FSRS, we have only examined the time-dependence of FSRS signal intensities for $\Delta t > 2$ ps where k is relatively constant and have only examined the time-

dependence of peak positions and shapes on faster timescales. A plot of time-dependent values m and k is provided in the supplementary material.[35]

Our primary concern in this work is the wavelength- and time-dependent frequency of the C=C stretching band, the most intense band observed in the excited-state Raman spectra. It is important to note that alternate analysis procedures were also used to double-check that time-dependent frequency shifts in Raman spectra were not artifacts from the procedure described above.[35] Importantly, all methods applied give comparable results, with absolute peak positions negligibly affected by choice of analysis procedure and revealing the same wavelength- and time-dependent trends. These similarities indicate that quantitative conclusions we draw from our data are robust and are not tied to details of our analysis procedures.

D. Computational methods

A small set of DFT calculations were performed to support interpretation of spectra. All calculations were carried out in the Gaussian 09 software package.[38] All geometry optimizations were performed without symmetry constraints and utilized the 6-31G(d) basis set[39,40] along with the range-corrected CAM-B3LYP density functional.[41] Range-corrected functionals are necessary to correctly describe the Raman dispersion effect with increasing oligomer length.[42] All calculations were performed in vacuum. Stable geometries were verified by vibrational analysis that returned zero normal modes with imaginary frequencies. Reported vibrational frequencies are unscaled. The in-phase and out-of-phase C=C backbone stretches were identified by the distinctive intense Raman signal of the in-phase mode in conjunction with visual inspection of the normal mode motions using the Jmol software package.[43] Vertical electronic excitation energies and geometry-relaxed (optimized) excited singlet states were determined using time dependent density functional theory (TD-DFT), although vibrational analysis of the geometry optimized excited states could not be performed analytically or numerically as a result of the computational cost. Images of optimized geometries were generated using the Molekel version 5.4.0.8 software package.[44]

III. RESULTS

A. Steady-state spectroscopy of PCMT

To our knowledge, the photophysics and spectroscopy of PCMT have not been characterized, and we therefore present the steady-state absorption and Raman spectroscopy of this polymer – with instructive comparisons to related oligomers and polymers – prior to presenting results of time-resolved absorption and Raman measurements.

Figure 2 compares the steady-state UV/Vis absorption spectrum of PCMT dissolved in THF with spectra of dithiophene (2T) and terthiophene (3T) in dioxane, as well as RR-P3HT in chlorobenzene. UV-Vis data for the oligothiophenes were digitized from Ref. 20. Two features can be identified in the spectrum of each species; these include a low-energy band with a peak position dependent on the identity of the species, and a high-energy feature that appears near 250 nm for all systems. The lower-energy feature corresponds with the lowest energy π-π^* (S_0-S_1) transition.[20,45] The peak positions of the low-energy transition (ground-state absorption, or GSA) for these species are summarized in Table I together with GSA peak positions for quaterthiophene (4T), quinquethiophene (5T), and sexithiophene (6T).[20] It is well known that the GSA red-shift with oligomer length can be rationalized using a free-electron model,[20,45,46] which treats the π electrons of the conjugated systems as a one-dimensional free-electron gas (i.e., "particle in a box") that extends along the length of the oligomer chain. Based on the size-dependence of the electronic band gap of oligothiophenes, it has been estimated that the effective chromophore or conjugation length (the dominant segment length prepared via excitation) of RR-P3HT is ~7–10 monomers.[20] On the contrary, a similar comparison based only on length dependence of the chromophore (Fig. 2 and Table I) suggests that the effective conjugation length of PCMT is on the order of 2-3 monomers.

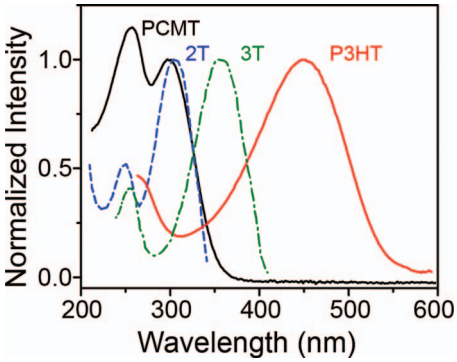

FIG. 2. Steady-state absorption spectra of poly-(3-cyclohexyl-4-methylthiophene) (PCMT) in THF, dithiophene (2T) and terthiophene (3T) in dioxane, and regioregular poly-(3-hexylthiophene) (RR-P3HT) in chlorobenzene. 2T and 3T spectra were taken from Ref. 20. Spectra are normalized to the peak of the lowest-energy transition for clarity.

Figure 3 compares the ground-state Raman spectra of PCMT and RR-P3HT. Mode-specific assignments for features in both spectra are based on those described in Refs. 12 and 26. The dominant feature at 1475 cm^{-1} for RR-P3HT is assigned to the in-plane, in-phase C=C ring stretching mode, whereas the weaker features at 1380 and 1525 cm^{-1} correspond with C_3-C_4 intra-ring and out-of-phase C=C stretch-

TABLE I. Peak positions for ground-state absorption (GSA), ground-state Raman (GSR), singlet transient absorption (STA), and triplet transient absorption (TTA) of PCMT, P3HT, and various oligothiophenes in solution. (GSA, STA, and TTA peak positions for 2T-6T were taken from Ref. 20. The STA and TTA peak positions of RR-P3HT is taken from Ref. 12. GSR peak positions of oligothiophenes are from Ref. 47.)

	2T	3T	4T	5T	6T	P3HT	PCMT
GSA/nm	306	355	392	414	435	455	298
GSA/eV	4.05	3.49	3.16	3.00	2.85	2.73	4.16
GSR (C=C)/cm^{-1}	...	1463	1465	1467	1469	1475	1506
STA/nm	495	600	710	845	900	>1100	660
TTA/nm	...	460	560/595	630	680	885	580

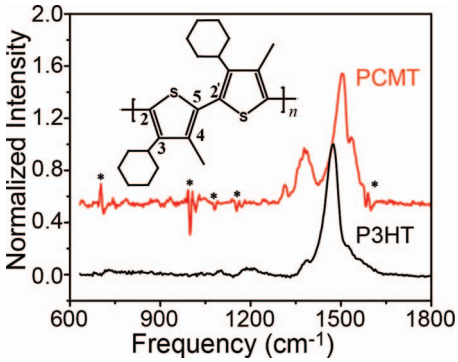

FIG. 3. Ground-state Raman (GSR) spectra of PCMT and RR-P3HT. Spectra were collected using 400 nm and 480 nm Raman excitation for PCMT and RR-P3HT, respectively. Asterisks denote artifacts from the subtraction of solvent bands. Spectra have been normalized to the peak of the in-phase C=C stretching feature and the GSR spectrum of PCMT is offset for clarity. The inset shows the structure of a dimeric unit of PCMT with labeled carbon sites.

ing of thiophene units (see Fig. 3 inset for carbon positions). For PCMT, features associated with the C=C in-phase and out-of-phase stretching modes appear at 1506 and 1534 cm^{-1}, respectively, as does an intra-ring C–C stretch at 1380 cm^{-1}. A weak feature appears near 1200 cm^{-1} for P3HT and corresponds with the inter-ring C_2–$C_{5'}$ stretch; in contrast, no clear feature can be distinguished from the baseline in this region for PCMT in light of artifacts from solvent-feature subtractions and a lower signal-to-noise ratio.

B. Excited-state dynamics of PCMT probed with broadband TAS

Transient spectral dynamics of PCMT were initiated with a photoexcitation (actinic) wavelength of 320 nm in order to cleanly excite only the lowest-energy electronic transition of the polymer (see Fig. 2). Figure 4 illustrates the transient spectral dynamics of PCMT as probed via absorption at visible wavelengths; this plot shows spectral evolution against a nonlinear time axis in order to highlight the spectral evolution that dominates each time regime of excited-state relaxation.

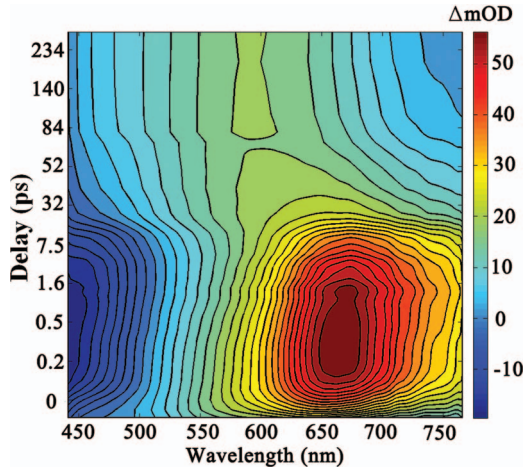

FIG. 4. Transient absorption spectroscopy (TAS) of PCMT in THF probed at visible wavelengths following photo-excitation at 320 nm.

Throughout the first 20 ps that follow photoexcitation the transient spectrum of PCMT can be characterized as the superposition of a negative feature below 520 nm and a positive band that peaks around 660 nm. Because the ground-state absorption of PCMT falls much further to the blue (Figure 2, solid black line), the negative band appearing in the transient spectrum must correspond with stimulated emission (SE) from the transient excited state rather than a bleach of the ground-state absorption. On the other hand, the positive band corresponds with a transition to a higher-lying excited state of the polymer. Two distinct spectral dynamics associated with these features are apparent from Figure 4: (1) Disappearance of these features with the concomitant appearance of a broad and weaker absorption peaking at 600 nm on a 10 s of picoseconds timescale, which signals decay out of the initially prepared excited state; and (2) an initial shift in the transient spectrum of the photoprepared excited state on sub-ps to picosecond timescales.

1. Intersystem crossing dynamics

The spectral evolution occurring on longer timescales (process 1 listed above) is similar to what has been observed previously in picosecond time-resolved studies of excited oligothiophenes:[20,48–50] For oligomers, spectral evolution over tens to hundreds of picoseconds is dominated by the disappearance of the singlet transient absorption (STA) and SE bands and the appearance of a broad absorption centered at shorter wavelengths that is attributed to a triplet transient absorption (TTA); assignment of this weaker band to a triplet state is predicated on its sensitivity to the presence of common triplet quenchers.[20] Peak wavelengths for STA and TTA of various oligothiophenes are listed in Table I along with the peak positions of transient spectra observed for PCMT in Fig. 4. This similarity with the spectral dynamics of oligothiophenes indicates that the photophysics of the lowest singlet excited state of PCMT is dominated by intersystem crossing to a longer-lived triplet level.

To further characterize these dynamics we have analyzed the excited-state spectral evolution over time delays >4 ps using principle component (PCA) and global target analysis.[51,52] Figure 5(a) plots spectral cuts from Fig. 4 at selected delays after 4 ps (solid lines). Spectra collected on times below 4 ps were excluded from this analysis in order to eliminate the influence of fast spectral shifting (process 2 above) on these analyses. PCA was used to determine that only two significant components contribute to the spectral evolution over this time regime, which is consistent with the presence of the isosbestic point at 585 nm in Fig. 5(a). Global target analysis was then applied using a sequential, two-state kinetic interconversion model ($S_1 \rightarrow$ triplet) in order to obtain the S_1 lifetime, τ_{S1}, and spectra of the two photophysical species. Importantly, only τ_{S1} was adjusted to fit the data in a least-squares minimization of the differences between the model and data.

The spectra of the two photophysical components obtained from global target analysis are plotted in Figure 5(b). Dashed lines in Fig. 5(a) plot the reconstructed time-dependent spectra obtained using this simple kinetic model,

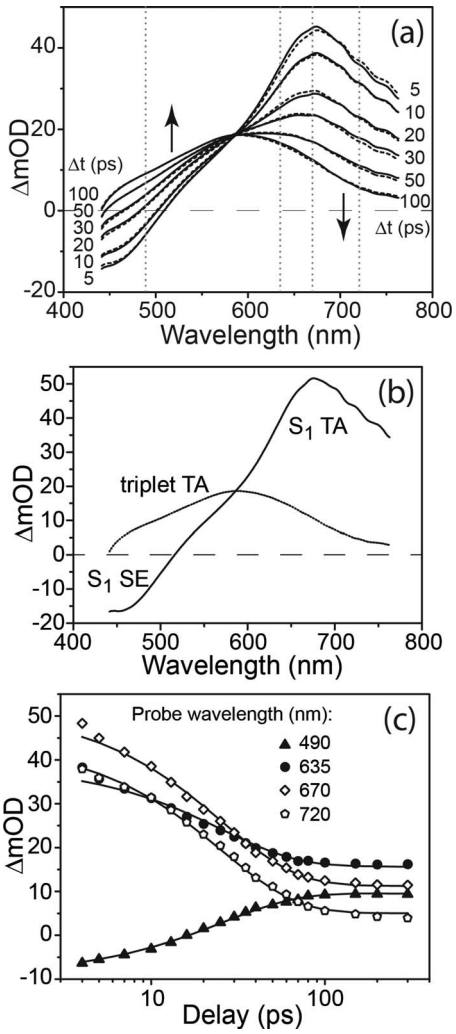

FIG. 5. Global target analysis of PCMT transient absorption on times >4 ps. (a) Experimental spectra (solid lines) compared to spectra obtained via fitting to a kinetic interconversion model (black dashed lines). (b) Component spectra obtained from global target analysis: S_1 transient absorption and stimulated emission, and triplet transient absorption. (c) Transient absorption (symbols) with fits to kinetic model (solid lines) at the selected wavelengths denoted with gray dotted lines in panel (a); data are plotted logarithmically with time to demonstrate the quality of the kinetic fit over all timescales.

the associated component spectra, and the value of τ_{S1} that minimizes the sum of squared residuals with the experimental data. Time-dependent intensities at selected probe wavelengths are plotted in Figure 5(c), along with curves corresponding with the kinetic interconversion model applied (solid lines); we have plotted these on a logarithmic time axis to highlight the quality of the fits over the entire range of delays. The fit to the data on these timescales is quite good, and yields an S_1 lifetime of 25.6 ps. The component spectra of the singlet and triplet states obtained are similar to corresponding spectra for oligomers.[35]

2. Ultrafast TA spectral relaxation

On much shorter timescales, transient spectral features from the photoprepared singlet excited state are observed to red-shift by ~25 nm during the first several hundred femtoseconds after excitation. This fast evolution is most apparent in Figure 6 (inset), in which the transient singlet spectra measured over the first 260 fs have been normalized such that they have the same peak intensity. The time-dependent peak position of the singlet absorption band is plotted up to the first 10 ps after excitation. Experimental data has been fitted using a bi-exponential function with two relaxation timescales:

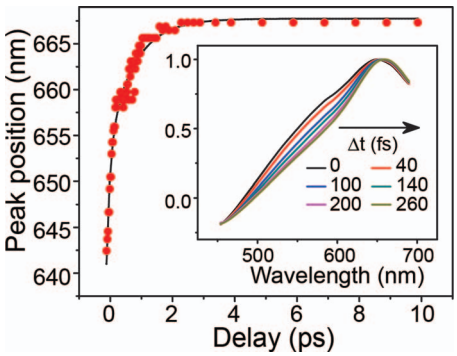

FIG. 6. Time-dependent shift in the S_1 transient absorption peak position; the solid line corresponds with a biexponential fit to the peak position explained in the text ($\tau_1 = 110 \pm 20$ fs, $\tau_2 = 800 \pm 100$ fs). (Inset) Peak-normalized pump-probe spectra of PCMT illustrate spectral evolution occurring over the first few hundred fs.

$$\lambda_{peak}(t) = \Delta\lambda_1 \exp\left(-\frac{t}{\tau_1}\right) + \Delta\lambda_2 \exp\left(-\frac{t}{\tau_2}\right) + \lambda_{peak}^{final}. \quad (3)$$

A fit to this function yields two relaxation timescales, 110 ± 20 fs and 800 ± 100 fs (fit shown with a dashed line).

C. Excited-state relaxation of PCMT probed with FSRS

1. Intersystem crossing

On longer time delays ($t >$ a few picoseconds), excited-state Raman spectroscopy provides a complementary probe of ISC that follows the photoexcitation of PCMT.

Figure 7 presents time-dependent excited-state Raman spectra obtained with (a) 840 and (b) 600 nm Raman-excitation pulses following 320-nm excitation of PCMT. Transient absorption of the singlet extends into the near IR (not shown in Figs. 4 and 5(a)),[35] whereas the TTA band is limited to the visible region of the spectrum; thus Raman excitation at 840 nm enables state-selective interrogation of the photoprepared singlet state via resonance enhancement. Figure 7(a) demonstrates that the resonance enhanced Raman at 840 nm gives rise to a single set of Raman features that decay with delay following the photopreparation of the excited singlet state. In contrast, Raman excitation at 600 nm enables resonance enhancement with both the STA and TTA bands, and thus probes vibrational signatures of both the singlet and triplet states through the course of ISC. Spectra collected with 600-nm Raman excitation for representative delays >2ps are plotted in Figure 7(b) (solid lines). Much like absorption transients shown in Figure 5, Raman transients exhibit signatures of a kinetic interconversion, with an isosbestic point appearing near 1460 cm^{-1}.

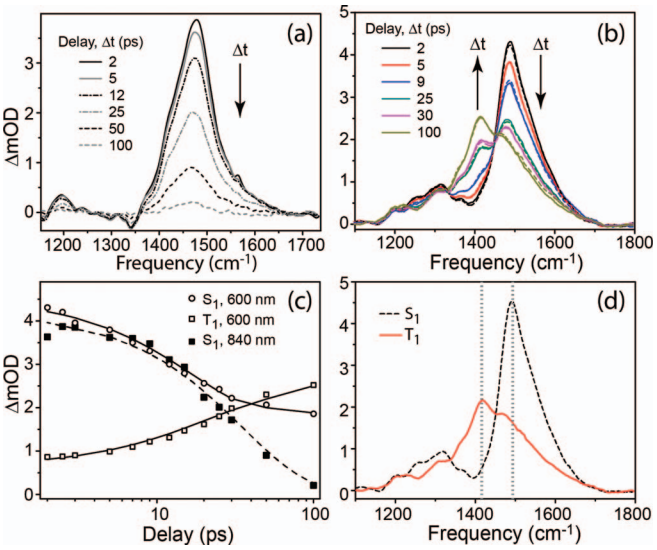

FIG. 7. Time-resolved resonant-Raman spectroscopy of PCMT in THF. (a) 840-nm Raman excitation selectively probes S_1 PCMT. (b) 600-nm Raman excitation probes both the S_1 and triplet states: Data, solid lines; fits from global analysis, dashed lines. (c) Time-dependence of peak intensity of S_1 and triplet features. Solid lines correspond with best-fit kinetic model obtained by global target analysis of data in (b); the dashed line corresponds with a single-exponential fit of Raman signal decay at 840-nm excitation. (d) Component S_1 and triplet Raman spectra obtained from global analysis of transient Raman probed via 600-nm Raman excitation.

We have applied global target analysis to the time-dependent Raman spectra obtained with 600-nm resonant excitation; the kinetic model applied here was identical to that used in our analysis of TAS data. Dashed lines in Fig. 7(b) correspond with the reconstructed time-dependent spectra obtained with a two-component model, with Raman spectra for the singlet and triplet states plotted in Figure 7(d). Minimizing the sum of residuals squared resulted in a τ_{S1} of 18 ps, which is somewhat faster than that obtained from TAS data. Temporal cuts through the time-dependent spectra taken near the peaks of the singlet and triplet features at 1493 and 1421 cm^{-1}, respectively, are plotted in Figure 7(c) (open symbols) along with the best fit curves obtained through global target analysis. The time-dependent intensity of the singlet vibrational spectrum obtained using 840-nm Raman excitation is also plotted in this panel (solid circles); fitting these to an exponential decay gives a singlet decay timescale of 33 ± 2 ps.

The discrepancies in intensity-dependent decay amongst all three measurements (1 TAS and 2 FSRS) could be associated with inaccuracies in the estimation and subtraction of baseline contributions to regions congested with broad Raman features or variations in the excited-state population available to probe due to interactions with the Raman-pump pulse. One might also expect that an all-parallel FSRS geometry would result in faster decay lifetimes compared to magic angle TAS, as the FSRS geometry will be sensitive to time-dependent evolution in polarization anisotropy. This could explain the faster decay of FSRS signal at 600 nm, and the differences between the decay rates observed at the two Raman excitation wavelengths could be due in part to energy transfer from high- to low-energy sites along the polymer (see Sec. IV). However, we also anticipate that the ensemble of S_1 PCMT created via 320-nm photoexcitation should be characterized by a distribution in delocalization lengths (see Sec. IV), such that this discrepancy in lifetimes quite likely reflect the selectivity with which resonance Raman interrogates sub-populations characterized by different conjugation lengths and ISC rates. Indeed, the S_1 lifetime measured using only near-IR TAS (830–1100 nm) is 32 ± 1 ps, compared to 25.6 ps in the visible region.[35] Nevertheless, these various pieces of time-dependent data provide a consistent picture of the excited-state relaxation of the initially prepared excited singlet of PCMT via intersystem crossing.

The spectra plotted in Figure 7(a), 7(b), and 7(d) share many similarities with Raman spectra of polythiophenes in their ground and excited states. Feature assignments can be made through comparisons with the PCMT ground-state Raman spectrum, the P3HT excited-state Raman spectrum, and the Raman spectra of oxidized thiophenes.[12,26,53] For the singlet excited state, the feature at 1490 cm^{-1} can be attributed to C=C stretching; this feature is quite broad and asymmetric in shape, and likely includes contributions also from intra-ring C–C stretching at frequencies slightly to the red of the peak and (intra-ring) out-of-phase C=C stretching at slightly higher frequencies (see Fig. 3). Raman features near 1200 cm^{-1} are attributed to inter-ring stretches. Raman intensity also appears near 1300 cm^{-1}; the relative intensity appears to decrease when probing via low-energy Raman excitation, although this may be (in part) due to differences in quality of the baseline removal in this region of the spectrum. The C=C stretching region of the triplet is red-shifted considerably relative to that of the singlet. Peak positions are consistent with so-called "quinoidal" stretching frequencies observed in the Raman spectra of oxidized polythiophenes.[53]

2. Ultrafast nuclear dynamics

Whereas time-dependent Raman spectra measured on time delays of picoseconds provide a complementary perspective on the ISC dynamics captured via TAS, evolution of Raman spectra on ultrafast timescales provide a new perspective on the nuclear dynamics that accompany the initial relaxation of the polymer after excitation. Figure 8 plots Raman spectra collected at delays within the first 200 fs after photoexcitation for the two Raman excitation wavelengths. Spectra have been normalized to the peak of the C=C stretching feature in order to directly compare peak positions and feature shapes. At both excitation wavelengths the peak position of the Raman features is observed to redshift over the first 150 fs. Furthermore, the band in the C=C stretching region is observed to narrow considerably on this same timescale when probing via resonance at 600 nm (Fig. 8(a)).

Figure 9(a) summarizes the time-dependence in the peak positions of C=C stretching bands measured at the two Raman-excitation wavelengths. In order to rule out the possibility that the specifics of the baseline subtraction procedure influences the extracted peak positions, we have verified that these trends are still observed when minimal data processing is applied.[35] Results obtained using both methods are almost identical, demonstrating that spectral manipulations required

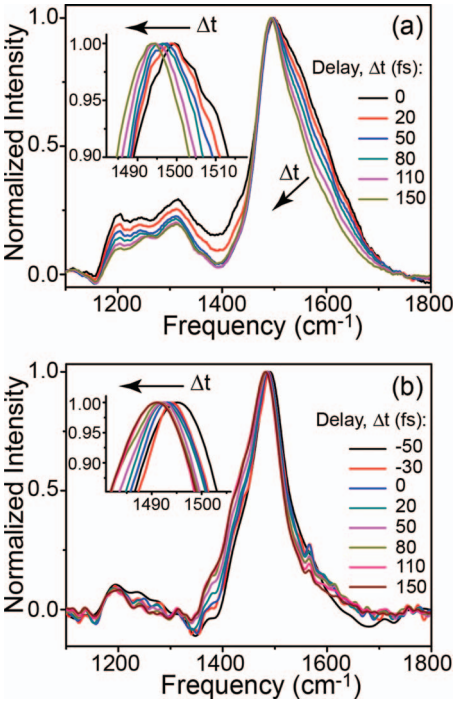

FIG. 8. Ultrafast evolution in Raman features of S_1 PCMT after 320-nm excitation. (a) 600-nm and (b) 840-nm Raman excitation. (Inset) Blow-up of the C=C peak-shift with delay.

for analysis do not affect the position assignments. In fact, the trends in peak position are discernible directly from raw FSRS data.

The excited-state Raman peak positions presented in Figure 9(a) exhibit two behaviors. Firstly, a shift in the C=C stretching frequency is identified between spectra collected

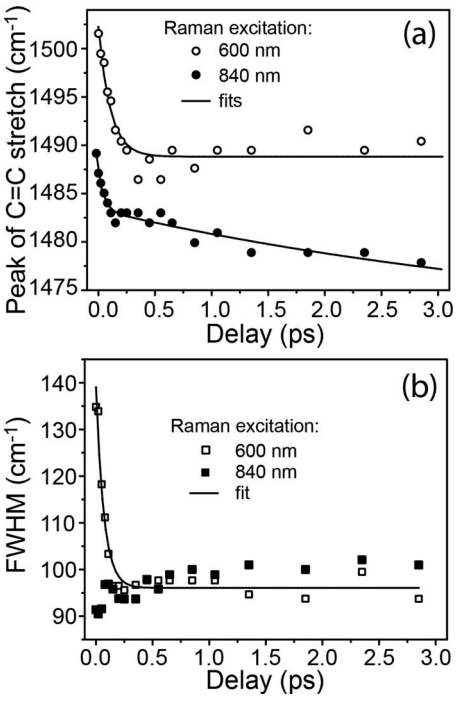

FIG. 9. Spectral evolution in the C=C stretching region for S_1 PCMT after 320-nm excitation. (a) Time-dependent Raman peak position as probed via 600 nm and 840 nm Raman excitation. (b) FWHM of the C=C stretching region.

at the two Raman excitation wavelengths at any given delay, with the stretching frequency falling ~10–15 cm^{-1} lower when probing with a lower Raman-excitation energy. A second observation is that the peak positions shift to lower frequency with time at both Raman excitation energies. The Raman frequency probed via 600-nm Raman excitation exhibits a 110 ± 10 fs shifting timescale while the C=C frequency probed with 840 nm shifts on two timescales at 80 ± 20 fs and 2.2 ± 0.5 ps; these timescales were determined by fitting the peak position to mono- and biexponential shifting function similar to Equation (3).

Figure 9(b) plots the time-dependent evolution in the width of the band in the C=C stretching region. Time-dependence in the FWHM of the C=C stretching bands shows contrary behavior at the two excitation wavelengths: The bandwidth decreases over the first ~200 fs when probed via a 600-nm excitation pulse, but is roughly constant under 840-nm Raman excitation. In order to verify that these changes are real and not an artifact of baseline subtraction, spectra were analyzed with an alternative baseline-correction method.[35] The evolution in feature bandwidth measured with 600-nm Raman excitation occurs on a timescale of 90 ± 10 fs timescale (fit with a solid line in Fig. 9(b)), which is similar to timescales obtained for the shift in peak position. Figure 8(a) demonstrates that this evolution in bandwidth occurs from changes to the band shape on the blue side of the spectrum between 1500 and 1650 cm^{-1}, which overlaps the region of the C=C in-plane out-of-phase stretching mode.

IV. DISCUSSION

A. Steady-state spectroscopy and the ground-state geometry of PCMT

A comparison of the absorption spectrum of PCMT in its ground state with the spectra of oligothiophenes (Fig. 1 and Table I) predicts an effective delocalization length for its ground state of 2–3 monomer units. A critical caveat about this comparison is that the substituents and associated steric interactions between monomer units in the polymer can be expected to influence ring-to-ring dihedral angles and should give rise to a larger vertical gap to the potential-energy surface of the quasi-planar excited-state in the Franck-Condon region when compared to unsubstituted oligothiophenes.[54,55] Explained at the level of the free-electron model, an increase of dihedral angle will increase the energetic asymmetry between the limiting valence-bond structures and thus the periodic potential that describes the degree of bond-length alteration.[46]

In order to qualify how much the dihedral angle influences the vertical excitation energy, we have calculated the lowest vertical transition energy for bithiophene at various dihedral angles. The ground state geometry was first optimized in the gas phase and a dihedral angle (C_3-C_2-$C_{5'}$-S, following the labels in Figure 3) of 26.1° was obtained at the minimum-energy geometry, which is very close to published experimental and theoretical results.[56–58] Constrained optimizations were then performed with the dihedral angle fixed to several different values, with corresponding energy gaps ($S_1 \leftarrow S_0$) determined at the TD/CAM-B3LYP/6-31G(d) level of the-

TABLE II. S_1 vertical transition energy of 2T as a function of inter-ring dihedral angle.

Dihedral	$S_1 \leftarrow S_0$ (eV)
0°	4.353
26.1°	4.507
50°	4.836
75°	5.353

ory. Results of these calculations are summarized in Table II and illustrate that the band gap of 2T increases by ∼1 eV when the dihedral angle is modified from 0° to 75°. This dependence on torsion dihedral is comparable to the difference in energy gap between oligomers in this size regime (e.g., 2T vs. 3T),[20] and thus we can conclude that an effective conjugation length of 2–3 monomers is not highly dependent on the torsional order of the polymer. Compared with oligothiophenes and P3HT, the dihedral angle of PCMT can be expected to be larger due to large steric interactions between the substituents on adjacent thiophene rings. Indeed, a ground-state geometry optimization of a 3-cyclohexyl,4-methylthiophene dimer (2-CMT) using these same calculation methods predicts a torsional dihedral of 82°. Such an extreme dihedral angle for PCMT would explain the slightly larger transition energy for PCMT (4.16 eV) compared to 2T (4.05 eV).

Steady-state Raman measurements reveal a significant shift in the in-phase C=C stretching frequency between PCMT and P3HT. Another critical difference is the relative intensity of the in-phase and out-of-phase C=C stretching features. DFT calculations were undertaken with simple oligomer analogues of P3HT and PCMT in order to relate these observations to differences in molecular structure. These analogues included a tetramer of 3-methylthiophene (3′,3″,3‴,3⁗-tetramethyl-2,2′:5′,2″:5″,2‴-quaterthiophene, herein referred to as 4-MT), serving as a computationally tractable model of P3HT, and a tetramer of 3,4-dimethylthiophene (3,3′,3″,3‴,4,4′,4″,4-octamethyl-2,2′:5′,2″:5″,2‴-quaterthiophene, herein referred to as 4-DMT), serving as a model for PCMT. Key results from these calculations are reported in Table III.

The effect of the second methyl substituent on the ground-state tetramer structure is readily apparent, with the average inter-ring dihedral angle (θ) increasing by 40° from 4-MT to 4-DMT. The large dihedral angle for 4-DMT is also consistent with the large dihedral for 2-CMT mentioned above. Comparing the calculated Raman spectra of 4-DMT to 4-MT, the in-phase C=C stretch blue-shifts by ∼40 cm^{-1} and the relative intensities of the out-of-phase to the in-phase C=C stretching mode increases from ∼10% to ∼20% with the introduction of the second methyl group on each monomer. Both findings are consistent qualitatively with Raman spectra previously calculated for 7T at various dihedral angles.[27] These calculated trends agree qualitatively with differences in the ground-state Raman spectroscopy of P3HT and PCMT. This implies that the larger steric interactions in PCMT increases the ground-state dihedral angle relative to P3HT and is responsible for both the increase in the in-phase C=C stretching frequency and the intensity increase in the out-of-phase C=C mode relative to the in-phase stretch.

TABLE III. DFT-calculated inter-ring dihedral angle (θ), in-phase C=C stretching frequency, and out-of-phase/in-phase C=C stretch intensity ratios for quaterthiophene analogues of P3HT and PCMT.

	θ	C=C stretch (cm^{-1})	$I_{out\text{-}of\text{-}phase}/I_{in\text{-}phase}$
4-MT	32°	1568	0.114
4-DMT	73°	1605	0.197

We have also calculated the minimum geometries for the S_1 excited states of 4-MT and 4-DMT in order to determine the magnitude of planarization that should be expected upon photoexcitation. For 4-MT the dihedral angle decreases from 32° to fully planar 0.0°, while for 4-DMT the dihedral angle decreases from 73° to 23°.[35] This implies that the magnitude of geometric relaxation after excitation in PCMT is considerably greater than in P3HT, and any experimental features arising from this relaxation should be more pronounced in PCMT as compared to P3HT.

B. Intersystem crossing in PCMT

The relatively fast ISC kinetics observed here following photoexcitation of PCMT are similar to the electronic relaxation dynamics of short oligothiophenes,[20,50,59–61] but contrast with the much slower ISC kinetics for P3HT and other polyalkylthiophenes with substituents only located at the C_3 site.[12] For oligothiophenes the rate of ISC has been observed to decrease substantially as the oligomer length is increased.[20] This variation in rate has been attributed to length-dependence in the relative energetics of states in the triplet and singlet manifolds modulated by state-to-state spin-orbit couplings between the S_1 and triplet levels:[45,61] At very short oligomer lengths (2T and 3T), the S_1 state lies relatively close energetically to higher-lying triplet states ($>T_1$) that couple strongly to the excited singlet, giving rise to correspondingly faster ISC rates. ISC occurs on a timescale of ∼50 ps for 2T, for which the lowest-lying excited singlet state is roughly isoenergetic with the T_2 level. In contrast, the S_1 level falls below the T_2 level for terthiophene.[61] Excitation-dependent ISC lifetimes were measured for 3T, decreasing from 126 to 51 ps between 400 and 374 nm,[60] as were energy-dependent triplet yields;[50] these results suggest increased singlet-triplet coupling as excitation tunes towards the higher-lying triplet level.[50] As the oligomer length is increased further (>4), the S_1 level drops even further below these triplet levels, and ISC rates occurring over several hundred ps or longer.[20,59] These variations in ISC rate with oligomer length may also be intimately tied to a length dependence of the intermonomer dihedral angle, which is thought to increase at smaller oligomer lengths. Such a relationship is well-known and supported by recent work with substituted phenylthiophenes that has demonstrated that ISC rates are directly sensitive to torsional dihedral angle.[62]

The ISC lifetime measured for PCMT is somewhat shorter than that of 2T in solution, further suggesting that the

effective delocalization length of the relaxed exciton in PCMT is on the order of 2–3 monomer units. More importantly, the substantially faster rate relative to other polythiophenes reflects that the relative energetics and/or coupling between singlet and triplet manifolds are highly sensitive to the torsional dihedral angle. Although the concept of an "effective conjugation length" provides a zeroth-order picture of localized states along conjugated polymers, delocalization length and energetics in polymers is not by nature limited by the physical length of the molecule as it is for oligomers. Thus, the observation of fast ISC dynamics in PCMT is a strong indicator that torsional conformation truly plays a significant role on ISC dynamics in oligo- and polythiophenes.

C. Variations in excited-state delocalization observed with transient absorption and wavelength-dependent Raman spectroscopies

Comparisons of transient absorption spectra obtained for PCMT with those of oligothiophenes in their relaxed excited states enables consideration of the extent of delocalization in polymer excited states. Excited-state peak positions of oligomer and polymer transient bands are summarized in Table I.[20,35] For oligomers the STA peak position shifts from 495 nm to 900 nm and the TTA peak position shifts from 460 nm to 680 nm as the chromophore length is increased from 2 to over 6 monomers. STA and TTA spectra of PCMT overlap with spectra of oligothiophenes over a range of lengths. Using a band-gap argument similar to that applied to the ground-state absorption spectrum of PCMT, one would estimate an effective conjugation length for relaxed singlet PCMT to be 2–5 monomers at 1 ps and a triplet conjugation length of 3-6 monomers at 1 ns. This comparison suggests that an ensemble of delocalization lengths are created after photoexcitation of PCMT, although the precise distribution in delocalization length for the ensemble of photoexcited PCMT cannot be assessed quantitatively from comparisons with unsubstitued thiophene oligomers for the same reasons described above in Sec. IV A.

As illustrated in Figures 8 and 9(a), the C=C stretching frequency measured for the relaxed PCMT excited state is dependent on the Raman-excitation wavelength. This likewise reflects that a distribution of excited-state delocalization lengths is prepared via photoexcitation, as C=C stretching frequencies and intensities are known to be directly sensitive to the extent of delocalization along the backbone of conjugated oligomers and polymers.[32,33,47,63] The most general explanation for length-dependent Raman frequencies is given by the Effective Conjugation Coordinate (ECC) Theory,[32,63] which describes how delocalization across multiple monomers influences the frequency of the so-called "conjugation coordinate," Я, which corresponds with the change in molecular geometry between limiting valence structures (such as benzoidal and quinoidal resonance structures for oligo- and polythiophenes) and which also coincides with C=C in-phase stretching. The vibrational force constant along the conjugation coordinate (and hence the C=C stretch) is influenced by coupling of modes and is thus sensitive to delocalization of electron density between monomer units: Delocalization gives rise to vibrational coupling between monomers both locally and non-locally, and has the net effect of softening the force constants for vibration along the conjugation coordinate, thus reducing the vibrational frequency of the C=C stretch.

Raman frequency "dispersion" amongst oligothiophenes of various lengths in their ground states is virtually nonexistent,[47] as monomer aromaticity effectively pins electron density locally and limits delocalization in the ground state.[33] However, we expect that there should be considerable Raman frequency dispersion with variation in the effective delocalization length of excited states as these states are highly delocalized by nature. In polymers, excited states are effectively localized within finite segments of the extended polymer framework that may vary in length, conformation, or structure at different sites.[16] Thus, wavelength-dependent resonant Raman frequency dispersion provides a probe of the relative delocalization of excitons within an ensemble of excited polymers.

Based on the wavelength-dependence of the C=C stretching frequency from our measurements, it is clear that 600-nm and 840-nm Raman excitation interrogate excited-state sub-populations characterized by somewhat different degrees of delocalization. Furthermore, the direction of the shift in Raman frequency is consistent with the variation in effective conjugation that can be deduced from comparisons to the vertical excitation energies of oligomers: Higher-energy Raman excitation probes sub-populations characterized by shorter effective conjugation length and low energy Raman excitation probes excitons with longer conjugation lengths. Thus, our Raman measurements indicate that the excited-state population of PCMT exhibits a distribution of conjugation lengths that underlie the broad width of the transient absorption.

Probe-dependent S_1 decay rates measured with TAS and FSRS are yet another reflection of the distribution in excited-state delocalization generated via excitation of an ensemble of PCMT in solution: A somewhat longer lifetime of 32 ± 1 ps is obtained from the decay of near-IR absorption transients compared to the findings from TAS data obtained by probing at visible wavelengths (Fig. 5);[35] this slightly longer lifetime matches that obtained from decay of Raman signals probed via 840-nm excitation. As described above, ISC rates are highly sensitive to delocalization length amongst small thiophene oligomers. Given the similarities between PCMT and oligothiophene photophysics, we expect that a distribution of delocalization lengths within PCMT would exhibit a corresponding variation in S_1 decay rate via ISC. As longer probe wavelengths (or Raman excitation wavelengths) interrogate longer conjugation lengths, we expect that the observed ISC rate should be slower when measured in these regions relative to a region of shorter wavelengths, explaining the wavelength-dependent ISC rates obtained from both our Raman and TAS measurements.

Finally, we note that the distribution in effective delocalization lengths in PCMT and the potential for energy transfer between them may explain differences observed in the FSRS signal decay measured at 600 and 840 nm using an all-parallel polarization geometry: Raman excitation at 600 nm presum-

ably interrogates shorter conjugation lengths from which energy transfer would originate; thus the somewhat faster FSRS signal decay relative to the magic angle TAS may reflect contributions from both population and polarization anisotropy decays. The 840-nm FSRS signal decays much more slowly with the same all-parallel polarization geometry, with a lifetime that matches the NIR decay measured by TAS at magic angle to within experimental error. This may reflect that the polarization anisotropy has been randomized at longer probing wavelengths as a consequence of energy transfer to these sites.

D. Ultrafast relaxation of S_1 PCMT from TA and Raman spectral dynamics

The ultrafast TA spectral dynamics apparent in Figures 4 and 6, through which both the transient SE and absorption bands red-shift on sub-ps timescales, indicate that PCMT in its S_1 state undergoes fast nuclear relaxation following photoexcitation into its Franck-Condon region. The dynamic shift in the STA peak position is similar to the spectral shifting dynamics observed with other polythiophenes shortly after photoexcitation,[3,4,10–12] although the overall timescale observed for PCMT is considerably faster, with no apparent relaxation on timescales of picoseconds. Nevertheless, these spectral dynamics are consistent with both the resonant energy transfer and localized torsional relaxation mechanisms that have been invoked to explain relaxation on the picoseconds timescale. Given the highly twisted structure of the polymer noted above, we expect that there is likely to be a higher driving force for relaxation through both mechanisms, and thus a larger relaxation rate, for PCMT relative to less twisted polymers assembled from monosubstituted monomer units (e.g., P3HT).[11,23]

Spectral shifting on timescales ~100 fs also appears in our TAS data (within our experimental time-resolution), although it is difficult to ascribe this to specific nuclear relaxation mechanisms using the TAS data alone, although reports on other conjugated polymers attribute dynamics on similar timescales to torsional conformational relaxation out of the Franck-Condon region.[3,4,9] The ultrafast Raman data presented in Figures 8 and 9 provide a new experimental perspective on the nuclear dynamics that occur in the first 200 fs after photoexcitation: On the earliest time delays probed, C=C stretching frequencies are observed to red-shift at both Raman-excitation wavelengths on a timescale of ~100 fs (also comparable with our experimental time resolution). The direction of this frequency shift is consistent with the evolution expected as the inter-ring dihedral angle is reduced, as demonstrated through the ground-state C=C stretching frequencies of variously substituted oligothiophenes in Table III. Additionally, the change in spectral bandwidth (and shape) observed when probing via 600-nm Raman excitation is consistent with a time-dependent change in the relative intensities of the C=C out-of-phase and in-phase stretching bands over the first 150 fs following photoexcitation. The decrease in the relative intensity of the out-of-phase stretching band likewise indicates an evolution in the dihedral angle between monomers following photoexcitation in the direction of a more planar excited-state geometry along the polymer backbone. Given these observations, we believe that the ultrafast vibrational dynamics observed here are reflections of the nuclear distortions that enable ultrafast self-localization of the excited-state after photoexcitation. The trigger for self-localization is the relaxation from the ground-state geometry to a more planar configuration within a specific segment of the polymer.

It is interesting to note that the C=C stretching frequency as probed via 840 nm continues to evolve on a 2-ps timescale, whereas the frequency measured at 600 nm does not. Furthermore, we do not observe the same evolution in band shape at 840 nm as we do at 600 nm. These differences are most likely tied with the size and/or conformational selectivity of resonant Raman spectroscopy: As noted above, high-energy Raman excitation (600 nm) will selectively probe excitons characterized by a large vertical excitation gap, which would be associated with a shorter delocalization length and greater degree of conformational disorder; lower Raman excitation energies, on the other hand, interrogate excited regions characterized by greater delocalization and/or higher conformational order. The lack of significant changes in the band shape at 840 nm indicates that this excitation wavelength already probes highly ordered states. On the other hand, as the vertical energy gaps for various effective conjugation lengths overlaps more appreciably at longer wavelengths,[35] the C=C stretching frequency probed via Raman excitation at 840-nm will be more sensitive to the slower phases of nuclear relaxation apparent in TAS data.

V. CONCLUSIONS

We have used a combination of TAS and FSRS spectroscopies to interrogate the electronic and nuclear relaxation of excited-states of poly(3-cyclohexyl,4-methylthiophene), or PCMT. TAS measurements have revealed similar spectroscopic signatures to those previously attributed to exciton localization, relaxation, and singlet exciton decay in related photoexcited conjugated polymers and oligomers. On the other hand, ultrafast Raman measurements present new experimental signatures of ultrafast nuclear dynamics: Specifically, ultrafast shifting of the C=C stretching frequency and the relative intensity of in-phase and out-of-phase C=C stretching intensities provide a sensitive vibrational reporter on ultrafast (~100 fs) vibrational distortion associated with exciton self-localization or trapping. We have also demonstrated that the in-phase C=C stretching frequency provides a spectroscopic handle for interrogating the degree of delocalization in an ensemble of relaxed conjugated polymers in their S_1 excited state given the selectivity achieved via resonance enhancement. In sum, we have shown that time-resolved resonance enhanced Raman spectroscopy can be utilized as a sensitive probe of structural dynamics and structural variation within an ensemble of photoexcited conjugated polymers.

ACKNOWLEDGMENTS

Financial support for this work was provided through research start-up funds from Johns Hopkins University. The

computational aspects of this research used resources of the National Energy Research Scientific Computing Center, which is supported by the Office of Science of the U.S. Department of Energy (DOE) under Contract No. DE-AC02-05CH11231. W.Y. gratefully acknowledges financial support from the Mary Lydston Kilpatrick Fellowship. The authors thank Tim Magnanelli for implementing the four-phase acquisition routine used for FSRS

[1]A. Facchetti, Chem. Mater. **23**, 733–758 (2011).
[2]S. Gunes, H. Neugebauer, and N. S. Sariciftci, Chem. Rev. **107**, 1324–1338 (2007).
[3]N. Banerji, S. Cowan, E. Vauthey, and A. J. Heeger, J. Phys. Chem. C **115**, 9726–9739 (2011).
[4]E. Busby, E. C. Carroll, E. M. Chinn, L. Chang, A. J. Moulé, and D. S. Larsen, J. Phys. Chem. Lett. **2**, 2764–2769 (2011).
[5]J. Clark, T. Nelson, S. Tretiak, G. Cirmi, and G. Lanzani, Nat. Phys. **8**, 225–231 (2012).
[6]E. Collini and G. D. Scholes, Science **323**, 369–373 (2009).
[7]J. Du, Z. Wang, W. Feng, K. Yoshino, and T. Kobayashi, Phys. Rev. B **77**, 195205 (2008).
[8]I. Hwang and G. D. Scholes, Chem. Mater. **23**, 610–620 (2011).
[9]N. P. Wells and D. A. Blank, Phys. Rev. Lett. **100**, 086403 (2008).
[10]N. P. Wells, B. W. Boudouris, M. A. Hillmyer, and D. A. Blank, J. Phys. Chem. C **111**, 15404–15414 (2007).
[11]S. Westenhoff, W. J. D. Beenken, R. H. Friend, N. C. Greenham, A. Yartsev, and V. Sundström, Phys. Rev. Lett. **97**, 166804 (2006).
[12]W. Yu, J. Zhou, and A. E. Bragg, J. Phys. Chem. Lett. **3**, 1321–1328 (2012).
[13]S. V. Frolov, Z. Bao, M. Wohlgenannt, and Z. V. Vardeny, Phys. Rev. Lett. **85**, 2196–2199 (2000).
[14]W. J. Beenken and T. Pullerits, J. Phys. Chem. B **108**, 6164–6169 (2004).
[15]B. J. Schwartz, Nat. Mater. **7**, 427–428 (2008).
[16]S. N. Yaliraki and R. J. Silbey, J. Chem. Phys. **104**, 1245–1253 (1996).
[17]W. Barford, D. G. Lidzey, D. Makhov, and J. H. Meijer, J. Chem. Phys. **133**, 044504 (2010).
[18]D. W. McCamant, P. Kukura, S. Yoon, and R. A. Mathies, Rev. Sci. Instrum. **75**, 4971–4980 (2004).
[19]E. Collini and G. D. Scholes, J. Phys. Chem. A **113**, 4223–4241 (2009).
[20]D. Grebner, M. Helbing, and S. Rentsch, J. Phys. Chem. **99**, 16991–16998 (1995).
[21]J. Guo, H. Ohkita, H. Benten, and S. Ito, J. Am. Chem. Soc. **132**, 6154–6164 (2010).
[22]G. D. Scholes, Annu. Rev. Phys. Chem. **54**, 57–87 (2003).
[23]W. Westenhoff, C. Daniel, R. H. Friend, C. Silva, V. Sundström, and A. Yartsev, J. Chem. Phys. **122**, 094903 (2005).
[24]J. L. Sauvajol, D. Chenouni, J. P. Lére-Porte, C. Chorro, B. Moukala, and J. Petrissans, Synth. Met. **38**, 1–12 (1990).
[25]S. Miller, G. Fanchini, Y. Y. Lin, C. Li, C. W. Chen, W. F. Su, and M. Chhowalla, J. Mater. Chem. **18**, 306–312 (2008).
[26]G. Louarn, M. Trznadel, J. P. Buisson, J. Laska, A. Pron, M. Lapkowski, and S. Lefrant, J. Phys. Chem. **100**, 12532–12539 (1996).
[27]W. C. Tsoi, D. T. James, J. S. Kim, P. G. Nicholson, C. E. Murphy, D. D. C. Bradley, and J. Nelson, J. Am. Chem. Soc. **133**, 9834–9843 (2011).
[28]Y. Q. Gao and J. K. Grey, J. Am. Chem. Soc. **131**, 9654–9662 (2009).
[29]M. Baibarac, M. Lapkowski, A. Pron, S. Lefrant, and I. Baltog, J. Raman Spectrosc. **29**, 825–832 (1998).
[30]S.-A. Chen and J.-M. Ni, Macromolecules **25**, 6081–6089 (1992).
[31]Y. Furukawa, J. Phys. Chem. **100**, 15644–15653 (1996).
[32]C. Castiglioni, M. Del Zoppo, and G. Zerbi, J. Raman Spectrosc. **24**, 485–494 (1993).
[33]V. Hernandez, C. Castiglioni, M. Del Zoppo, and G. Zerbi, Phys. Rev. B **50**, 9815–9823 (1994).
[34]S. Laimgruber, H. Schachenmayer, B. Schmidt, W. Zinth, and P. Gilch, Appl. Phys. B **85**, 557–564 (2006).
[35]See supplementary material at http://dx.doi.org/10.1063/1.4890326 for description of alternative data processing procedures, comparison of PCMT and oligothiophenes transient absorption spectra, transient absorption of PCMT probed in the near-IR, and molecular structures obtained from DFT calculations.
[36]M. Kloz, R. van Grondelle, and J. T. M. Kennis, Chem. Phys. Lett. **544**, 94–101 (2012).
[37]A. Weigel and N. P. Ernsting, J. Phys. Chem. B **114**, 7879–7893 (2010).
[38]M. J. Frisch, G. W. Trucks, H. B. Schlegel *et al.*, Gaussian 09, Revision B.01, Gaussian, Inc., Wallingford, CT, 2010.
[39]J. S. Binkley, J. A. Pople, and W. J. Hehre, J. Am. Chem. Soc. **102**, 939–947 (1980).
[40]M. S. Gordon, J. S. Binkley, J. A. Pople, W. J. Pietro, and W. J. Hehre, J. Am. Chem. Soc. **104**, 2797–2803 (1982).
[41]T. Yanai, D. P. Tew, and N. C. Handy, Chem. Phys. Lett. **393**, 51–57 (2004).
[42]P. J. Donohoo-Vallett and A. E. Bragg, "Computational investigation of the effects of side-chain and dihedral conformation on the Raman spectroscopy of conjugated oligomers" (unpublished).
[43]*Jmol: An Open-Sourced Java Viewer for Chemical Structures in 3D.*, 12.2.33, (2012). See http://www.jmol.org/.
[44]U. Varetto, *Molekel*, version 5.4.0.8, Swiss National Supercomputing Centre, Manno, Switzerland (2010).
[45]D. Beljonne, Z. Shuai, G. Pourtois, and J. L. Bredas, J. Phys. Chem. A **105**, 3899–3907 (2001).
[46]H. Kuhn, J. Chem. Phys. **17**, 1198–1212 (1949).
[47]A. Milani, L. Brambilla, M. Del Zoppo, and G. Zerbi, J. Phys. Chem. B **111**, 1271–1276 (2007).
[48]G. Lanzani, M. Nisoli, S. De Silvestri, and R. Tubino, Synth. Met. **76**, 39–41 (1996).
[49]W. Paa, J.-P. Yang, and S. Rentsch, Appl. Phys. B **71**, 443–449 (2000).
[50]J.-P. Yang, W. Paa, and S. Rentsch, Chem. Phys. Lett. **320**, 665–672 (2000).
[51]J. J. Snellenburg, S. P. Laptenok, R. Seger, K. M. Mullen, and I. H. M. van Stokkum, J. Stat. Softw. **49**, 1–22 (2012), available at http://www.jstatsoft.org/v49/i03.
[52]I. H. M. van Stokkum, D. S. Larsen, and R. van Grondelle, Biochim. Biophys. Acta **1657**, 82–104 (2004).
[53]F. Chen, G. Shi, J. Zhang, and M. Fu, Thin Solid Films **424**, 283–290 (2003).
[54]T. Benincori, G. Bongiovanni, C. Botta, C. Cerullo, G. Lanzani, A. Mura, L. Rossi, F. Sannicolò, and R. Tubino, Phys. Rev. B **58**, 9082–9086 (1998).
[55]W. J. Beenken and H. Lischka, J. Chem. Phys. **123**, 144311 (2005).
[56]M. Takayanagi, T. Gejo, and I. Hanazaki, J. Phys. Chem. **98**, 12893–12898 (1994).
[57]M. Andrzejak and H. Witek, Theor. Chem. Acc. **129**, 161–172 (2011).
[58]E. Stendardo, F. Avila Ferrer, F. Santoro, and R. Improta, J. Chem. Theory Comput. **8**, 4483–4493 (2012).
[59]H. Chosrovian, S. Rentsch, D. Grebner, D. U. Dahm, E. Birckner, and H. Naarmann, Synth. Met. **60**, 23–26 (1993).
[60]W. Paa, J.-P. Yang, M. Helbing, J. Hein, and S. Rentsch, Chem. Phys. Lett. **292**, 607–614 (1998).
[61]S. Rentsch, J. P. Yang, W. Paa, E. Birckner, J. Schiedt, and R. Weinkauf, Phys. Chem. Chem. Phys. **1**, 1707–1714 (1999).
[62]I. Zheldakov, J. M. Wasylenko, and C. G. Elles, Phys. Chem. Chem. Phys. **14**, 6211–6218 (2012).
[63]G. Zerbi, C. Castiglioni, and M. Del Zoppo, *Electronic Materials: The Oligomer Approach* (Wiley, 2008).